AIAA Aviation Forum and ASCEND co-located Conference Proceedings
21 - 25 July 2025, Las Vegas, Nevada
AIAA AVIATION FORUM AND ASCEND 2025

10.2514/6.2025-3157

Simulation of 3D Co-Flow Jet Wings with Circular End-Plates

Feihao Ding * Jaehyoung Jeon † Yan Ren ‡ Gecheng Zha §
Dept. of Mechanical and Aerospace Engineering
University of Miami, Coral Gables, Florida 33124

Abstract

This paper numerically investigates aerodynamic efficiency improvements for Co-Flow Jet (CFJ) wings using circular end-plates with two diameters: One Chord (1C) and Two Chord (2C). Circular plates are simple devices for mitigating tip vortex, and are particularly useful for high lift wings using coflow jet airfoils. The simulations were performed using a Reynolds-averaged Navier-Stokes (RANS) solver with the Menter Shear Stress Transport (SST) model. A 5th-order WENO scheme is utilized for the inviscid flux, and a 2nd order central differencing scheme is used for the viscous terms. Compared to the CFJ wings with no tip end-plates, the results show that CFJ wings equipped with one-chord diameter end-plates approximately increase the average C_L by 9.2%, C_L/C_D by 18.4%, $(C_L/C_D)_c$ by 18.3%, and $(C_L^2/C_D)_c$ by 31.1%. Compared to the CFJ wings using one chord end-plates, the results show that CFJ wings equipped with two chord end-plates improve the average C_L and C_L/C_D by 9.7% and 6.8%, respectively. The average $(C_L/C_D)_c$ and $(C_L^2/C_D)_c$ are increased by 10.5% and 22.8%, respectively. Overall, enlarging the end-plate diameter significantly enhances the aerodynamic performance of CFJ wings. This study indicated that CFJ wings with circular end-plates significantly enhances aerodynamic efficiency, offering a robust technique for increasing aerodynamic efficiency with a high cruise lift coefficient.

Nomenclature

CFJ	CoFlow jet
$FCFJ$	Flapped CoFlow jet
$AoA(\alpha)$	Angle of attack
β	Deflection angle
LE	Leading Edge
TE	Trailing Edge
s	Wing Span length
c	Profile chord

* Ph.D. Candidate
† Ph.D. Student
‡ Research Scientist, Ph.D., AIAA member
§ Professor, ASME Fellow, AIAA associate Fellow

U	Flow velocity
q	Dynamic pressure $0.5\,\rho\,U^2$
p	Static pressure
ρ	Air density
P	Pumping power
C_L	Lift coefficient $L/(q_\infty\,S)$
C_D	Drag coefficient $D/(q_\infty\,S)$
C_μ	Jet momentum coef. $\dot{m}_j\,U_j/(q_\infty\,S)$
Pc	Power coefficient $P/(q_\infty\,S\,V_\infty)$
$(C_L/C_D)_c$	CFJ wing corrected efficiency $C_L/(C_D$+Pc)
R_e	Reynolds number
M	Mach number
C_p	Constant pressure specific heat
γ	Air specific heats ratio
S	Planform area of the wing
T_t	Total temperature
P_t	Total pressure
H_t	Total specific enthalpy
$\dot{m}$	Mass flow across the pump
$_\infty$	Subscript, stands for free stream
$_j$	Subscript, stands for jet

1 Introduction

The rapidly growing global aviation transportation demands continuous improvement of aircraft efficiency. By optimizing designs to increase lift and reduce drag, engineers improve the efficiency of aircraft systems, leading to lower fuel consumption and extended ranges. A persistent challenge in aerodynamic design is managing tip vortices—spirals of airflow that form at the wingtips due to the pressure difference between the upper and lower wing surfaces. These vortices create induced drag, which reduces aerodynamic efficiency. Over time, researchers have developed wingtip treatments, such as winglets, that mitigate the strength of tip vortices, and thus the induced drag. Using winglets, a 20% reduction of induced drag and roughly 9% enhancement in lift-drag ratio is proven by Whitcomb at Langley's transonic pressure tunnel [1]. Helal et al. concluded that the blended winglet can increase the aerodynamic performance by 6% to 15% [2]. Overall, Winglets have proven successful in various applications, including commercial aircraft, due to their ability to improve lift-to-drag ratios. However, the typical up-bent winglets are not necessarily suitable for all wing configurations, such as flapped wings using CoFlow Jet active flow control, which is a new type of wings that have a large flap with CoFlow Jet (CFJ) embedded inside the flap. These types of wings are advantageous for vertical takeoff/landing aircraft to implement deflected slipstream to avoid tiltrotors, tiltwings, and lift-plus-cruise configurations [3, 4]. The CFJ flap could be deflected by 80° downward at hover and be fully retracted for cruise, making the flap have a large displacement. A circular end-plate installed at the tip could cover a large area of the large flap displacement. Hemke and Paul [5] show that the maximum C_D reduction in their experiment is about 30% by adding a one-chord diameter circular end-plate to unswept aircraft wings.

Active flow control (AFC) has emerged alongside passive flow control methods like winglets as a promis-

ing approach to enhancing aerodynamic efficiency, especially by increasing the maximum lift coefficient (C_{Lmax}). AFC achieves it by adding energy to the flow, often through techniques like blowing or suction, to suppress flow separation and improve airfoil circulation. However, implementing AFC in cruise flight conditions is challenging. For the AFC to be truly effective, the gains in C_L and aerodynamic efficiency must outweigh the additional energy consumption of the AFC system to ensure an overall efficiency improvement for the aircraft system.

One promising AFC technology with the potential to overcome this challenge and enhance cruise efficiency is the CoFlow Jet (CFJ) flow control airfoil [6, 7, 8, 9, 10, 11, 12, 13, 14, 15, 16, 17, 18, 19, 20, 21]. A series of small micro-compressor actuators pumping system is embedded inside the airfoil as shown in Fig. 1. For a CFJ airfoil, as shown in Fig. 1, a small amount of mass flow is drawn into the suction duct, pressurized by a pump, and then injected near the LE tangentially to the main flow. In comparison with the 2D baseline airfoil, Wang and Zha[22] show that the 2D CFJ airfoil can achieve a significantly higher cruise lift coefficient and aerodynamic efficiency, defined as

$$(\frac{C_L}{C_D})_c = \frac{C_L}{C_D + P_c} \tag{1}$$

Where Pc is the CFJ required power coefficient. However, for 3D wings with finite aspect ratios, studies have shown that CFJ can still maintain a high cruise lift coefficient (C_L) while the aerodynamic efficiency is dropped to the level of the baseline condition[23]. The cruise productivity efficiency of aircraft is introduced as a parameter that can provide a more holistic evaluation of aircraft performance [17]:

$$(\frac{C_L^2}{C_D})_c = \frac{C_L^2}{(C_D + Pc)} \tag{2}$$

The present study conducts a detailed numerical investigation of 3D CFJ airfoils with integrated end-plates and demonstrates that the addition of end-plates is an effective technique for enhancing the aerodynamic efficiency of CFJ wings.

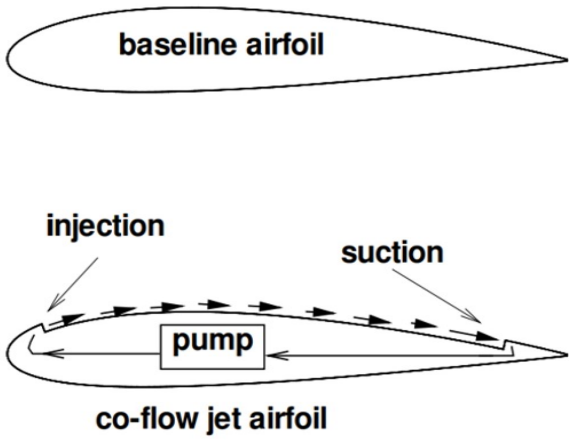

Figure 1: Sketch of CoFlow Jet airfoil

2 Methodology

2.1 Lift and Drag Calculation

The momentum and pressure at the injection and suction slots produce a reactionary force, which is automatically measured by the force balance in wind tunnel testing. However, for CFD simulation, the full reactionary force needs to be included. Using control volume analysis, the reactionary force can be calculated using the flow parameters at the injection and suction slot opening surfaces. Zha et al. [7] gives the following formulations to calculate the lift and drag due to the jet reactionary force for a CFJ wing. By considering the effects of injection and suction jets on the CFJ wing, the expressions for these reactionary forces are given as :

$$F_{x_{cfj}} = (\dot{m}_j V_{j1} + p_{j1} A_{j1}) * cos(\theta_1 - \alpha) - (\dot{m}_j V_{j2} + p_{j2} A_{j2}) * cos(\theta_2 + \alpha) \tag{3}$$

$$F_{y_{cfj}} = (\dot{m}_{j1} V_{j1} + p_{j1} A_{j1}) * sin(\theta_1 - \alpha) + (\dot{m}_{j2} V_{j2} + p_{j2} A_{j2}) * sin(\theta_2 + \alpha) \tag{4}$$

where the subscripts 1 and 2 stand for the injection and suction, respectively, and θ_1 and θ_2 are the angles between the injection and suction slot's surface and a line normal to the airfoil chord. α is the angle of attack.

The total lift and drag on the airfoil can then be expressed as:

$$D = R'_x - F_{x_{cfj}} \tag{5}$$

$$L = R'_y - F_{y_{cfj}} \tag{6}$$

where R'_x and R'_y are the surface integral of pressure and shear stress in x (drag) and y (lift) direction excluding the internal ducts of injection and suction. For CFJ wing simulations, the total lift and drag are calculated by integrating Eqs.(5) and (6) in the spanwise direction.

2.2 Jet Momentum Coefficient

The jet momentum coefficient C_μ is a parameter used to quantify the jet intensity. It is defined as:

$$C_\mu = \frac{\dot{m} V_j}{\frac{1}{2} \rho_\infty {V_\infty}^2 S} \tag{7}$$

where $\dot{m}$ is the injection mass flow, V_j is the mass-averaged injection velocity, ρ_∞ and V_∞ denote the free stream density and velocity, and S is the planform area.

2.3 Micro-compressor Power Coefficient

CFJ is implemented by mounting a pumping system inside the wing that withdraws air from the suction slot and blows it into the injection slot. The power consumption is determined by the jet mass flow and total enthalpy change as follows:

$$P = \dot{m}(H_{t1} - H_{t2}) \tag{8}$$

where H_{t1} and H_{t2} are the mass-averaged total enthalpy in the injection cavity and suction cavity respectively, P is the Power required by the pump and $\dot{m}$ the jet mass flow rate. Introducing P_{t1} and P_{t2} the mass-averaged total pressure in the injection and suction cavity respectively, the compressor efficiency η, and the total pressure ratio of the pump $\Gamma = \frac{P_{t1}}{P_{t2}}$, the power consumption is expressed as:

$$P = \frac{\dot{m} C_p T_{t2}}{\eta} (\Gamma^{\frac{\gamma-1}{\gamma}} - 1) \tag{9}$$

where γ is the specific heat ratio equal to 1.4 for air. The power coefficient is expressed as:

$$P_c = \frac{P}{\frac{1}{2}\rho_\infty V_\infty^3 S} \tag{10}$$

2.4 Aerodynamic Efficiency

The conventional wing aerodynamic efficiency is defined as:

$$\frac{C_L}{C_D} \tag{11}$$

For the CFJ wing, the ratio above still represents the pure aerodynamic relationship between lift coefficient and drag coefficient. However since CFJ active flow control consumes energy, the ratio above is modified to take into account the energy consumption of the micro-compressor. The formulation of the corrected aerodynamic efficiency for CFJ wings is:

$$(\frac{C_L}{C_D})_c = \frac{C_L}{C_D + P_c} \tag{12}$$

where P_c is the micro-compressor power coefficient defined in Eqn. 10 and C_L and C_D are the lift and drag coefficients of the CFJ wing. If the micro-compressor power coefficient is set to 0, this formulation returns to the aerodynamic efficiency of a conventional airfoil.

A productivity efficiency parameter was introduced by Yang et al[17]. It describes the capability to transport a gross weight for a maximum distance at cruise:

$$(\frac{C_L^2}{C_D})_c = \frac{C_L^2}{C_D + P_c} \tag{13}$$

2.5 CFD Simulation Setup

The FASIP(Flow-Acoustics-Structure Interaction Package) CFD code is used to conduct the numerical simulation. The 3D Reynolds Averaged Navier-Stokes (RANS) equations with the Menter Shear Stress Transport (SST) turbulence model are used. A 5th order WENO scheme for the inviscid flux [24, 25, 26, 27, 28, 29] and a 2nd order central differencing for the viscous terms [24, 28] are employed to discretize the Navier-Stokes equations. The low diffusion E-CUSP scheme used as the approximate Riemann solver suggested by Zha et al [25] is utilized with the WENO scheme to evaluate the inviscid fluxes. Implicit time marching method using Gauss-Seidel line relaxation is used to achieve a fast convergence rate [30]. Parallel computing is implemented to save wall clock simulation time [31].

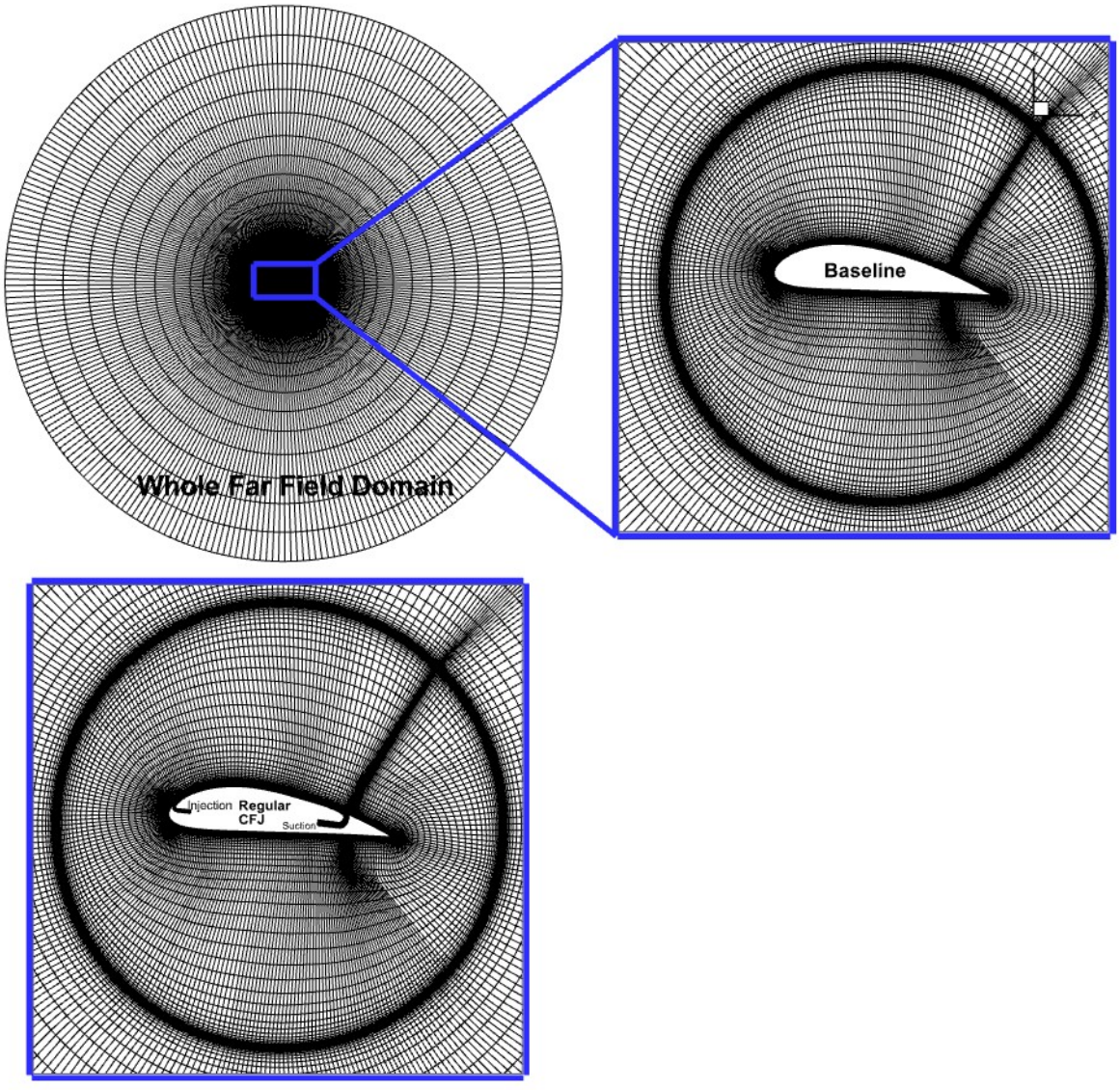

Figure 2: Computational mesh used in the current work.

2.6 Boundary Conditions and Mesh Analysis

The 1st-order accuracy no-slip condition is enforced on the solid surface with the wall treatment suggested in [32] to achieve the flux conservation on the wall. The far-field boundary is located at 55 chords with an O-mesh topology. The computational mesh is shown in Fig. 2. Total pressure, total temperature, and flow angles are specified at the upstream portion of the far field. Constant static pressure is applied at the downstream portion of the far field. The first grid point on the wing surface is placed at $y^+ \approx 1$.

2.7 Validations

A wing formed with airfoil NACA 64(1)-212, aspect ratio of 4, and circular end-plates installed at the wing tip is used to validate the simulation with the experimental data [33]. The Mach number is 0.211 and the Reynolds number is 1×10^6. Fig. 3 shows the flow field and Cp distribution of NACA 64(2)-212 baseline with one chord end-plates at AoA 10°. Near the leading edge, $-C_P$ has a maximum value with the highest flow velocity. The C_P at root, 50%, and 99% are almost identical after the leading edge. It validates the ability of end-plates to suppress the tip vortex. Additionally, the end-plates also eliminate the low momentum flow at the trailing edge at the tip of the wing section comparing with the flow fields at mid-span and root. The computed coefficients of lift and drag for the baseline wing with end-plates are in good agreement, as shown in Fig. 4. Very good agreement is achieved for both C_L and C_D except at high AoA of 14°, which has flow separation near trailing edge and the drag is over-predicted.

Another baseline wing with a thick NACA 6421 airfoil but with no end-plates is simulated and validated with the experiment [34]. The wing has an aspect ratio of 6 and was tested with a Mach number of 0.065 and a Reynolds number of 3.0×10^6. The CFJ airfoil is modified from the NACA6421 airfoil. Hence, this case shows the validation of the simulation for a wing with the same baseline thick airfoil. Since CFJ overcomes the tendency of flow separation caused by a thick airfoil and can achieve a very high stall angle of attack, such as greater than 60° [17] and obtains high cruise efficiency [20, 21], a thick CFJ airfoil is preferred to the advantages of high lift coefficient and lighter structure weight. The predicted C_L and C_D for the baseline wing with NACA 6421 airfoil are in excellent agreement with the experiment as shown in Fig. 5, demonstrating a high accuracy of the numerical approaches.

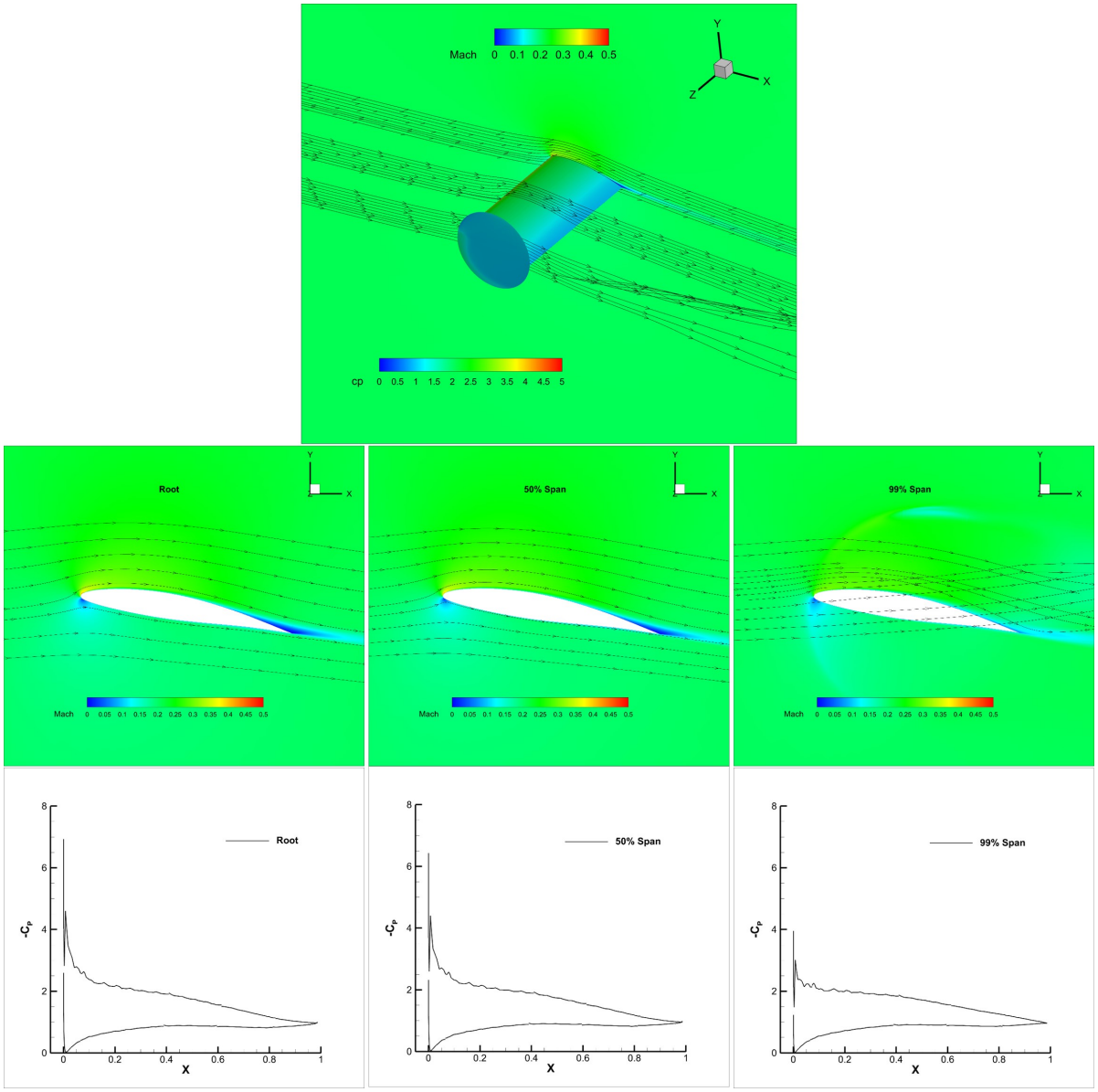

Figure 3: NACA 64(2)-212 with End-Plates flow field and pressure coefficient at $AoA = 10°$

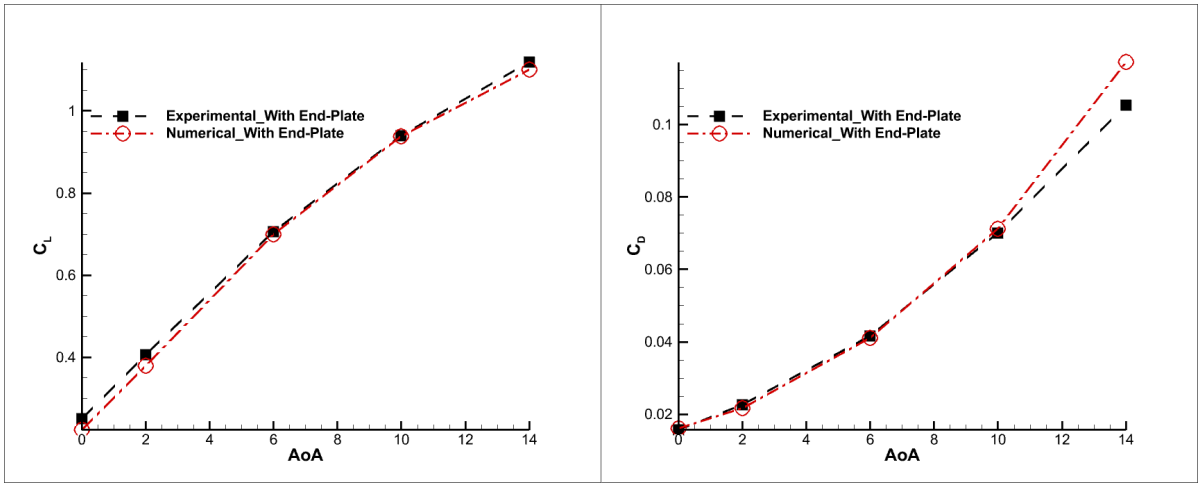

Figure 4: Comparison of C_L and C_D between experiment and computation of NACA 64(1)-212 with End-Plates at different AoA

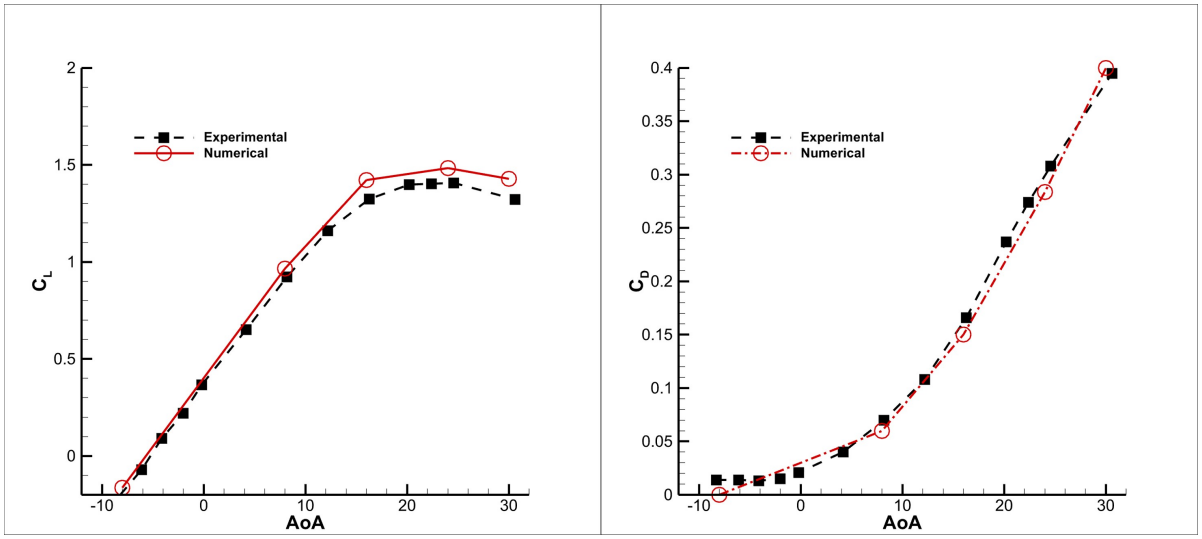

Figure 5: Comparison of C_L and C_D between experiment and computation of NACA 6421 at different AoA

2.8 Refinement Study

A mesh independence study is conducted for both meshes of NACA 64(1)-212 and NACA 6421 by doubling the number of grid points in $i-$, $j-$, and $k-$ directions respectively. Both cases were tested under the computational conditions of $Re_\infty = 1 \times 10^6$ and Mach $= 0.211$ at $AoA = 2°$, the mesh dependence results are shown in Table 1. The C_L and C_D variations are within 3% and thus the results are converged based on mesh sizes.

Table 1: Comparison of C_L, C_D of NACA 64(1)-212 and NACA 6421 at $AoA = 2°$

Airfoil Type	Case	Mesh Size	C_L	C_D
NACA 64(1)-212	Baseline	$280 \times 160 \times 100$	0.436	0.0344
	Doubled in i-direction	$560 \times 160 \times 100$	0.443	0.0353
	Doubled in j-direction	$280 \times 320 \times 100$	0.430	0.0348
	Doubled in k-direction	$280 \times 160 \times 200$	0.440	0.0347
NACA 6421	Baseline	$280 \times 160 \times 100$	0.788	0.0450
	Doubled in i-direction	$560 \times 160 \times 100$	0.788	0.0447
	Doubled in j-direction	$280 \times 320 \times 100$	0.788	0.0446
	Doubled in k-direction	$280 \times 160 \times 200$	0.787	0.0449

3 Results and Discussion

Three wing configurations are simulated and compared in this section: 1)the baseline NACA 6421 wing as shown in Fig. 2 with no end-plates, 2) a CFJ NACA 6421 wing designed by Wang and Zha [22] shown in Fig. 2 with no end-plates labeled as CFJ airfoil. 3) The CFJ wing with end-plates of 1C and 2C diameters. All the wings have the same aspect ratio of 4, freestream Mach number of 0.211, and Reynolds number of 1.0×10^6. The AoA range of 0° - 22° is simulated and compared to study the performance at cruise. Three C_μ values of 0.03, 0.06, and 0.08 have been simulated for the CFJ and the end-plates CFJ wings. Fig. 6 shows the results of C_L, C_D, P_C, C_L/C_D, $(C_L/C_D)_c$ and $(C_L^2/C_D)_c$ for all configurations at different C_μ values. The detailed values are listed in Table. 2, Table. 3, Table. 4, and Table. 5. Overall, the end-plates bring significant benefits. For the 1C end-plate, the average C_L is increased by 9.2%, C_L/C_D by 18.4%, $(C_L/C_D)_c$ by 18.3%, and $(C_L^2/C_D)_c$ by 31.1%. For the 2C end-plates, the average C_L is increased by 19.8%, C_L/C_D by 26.4%, $(C_L/C_D)_c$ by 30.8%, and $(C_L^2/C_D)_c$ by 61.0%.

3.1 Results for Baseline

Table. 2 presents the results for the NACA 6421 Baseline airfoils, demonstrating a maximum C_L of 1.221 and maximum C_L/C_D of 12.65 at very low angles of attack (AoA) of 2 deg. Even though the maximum C_L occurs at 18°, flow separation was observed after 4° as the C_L/C_D starts dropping. Fig. 7 illustrates the flow field and surface pressure coefficient at an AoA of 10° for baseline airfoils. A strong vortex is shown near the tip of the wing. The baseline wing has a flow separation at the trailing edge for the inner span, as shown by the Mach contours in Fig. 7. The separation is also reflected in the C_P distribution. At the tip, the loading is substantially reduced due to the tip vortex.

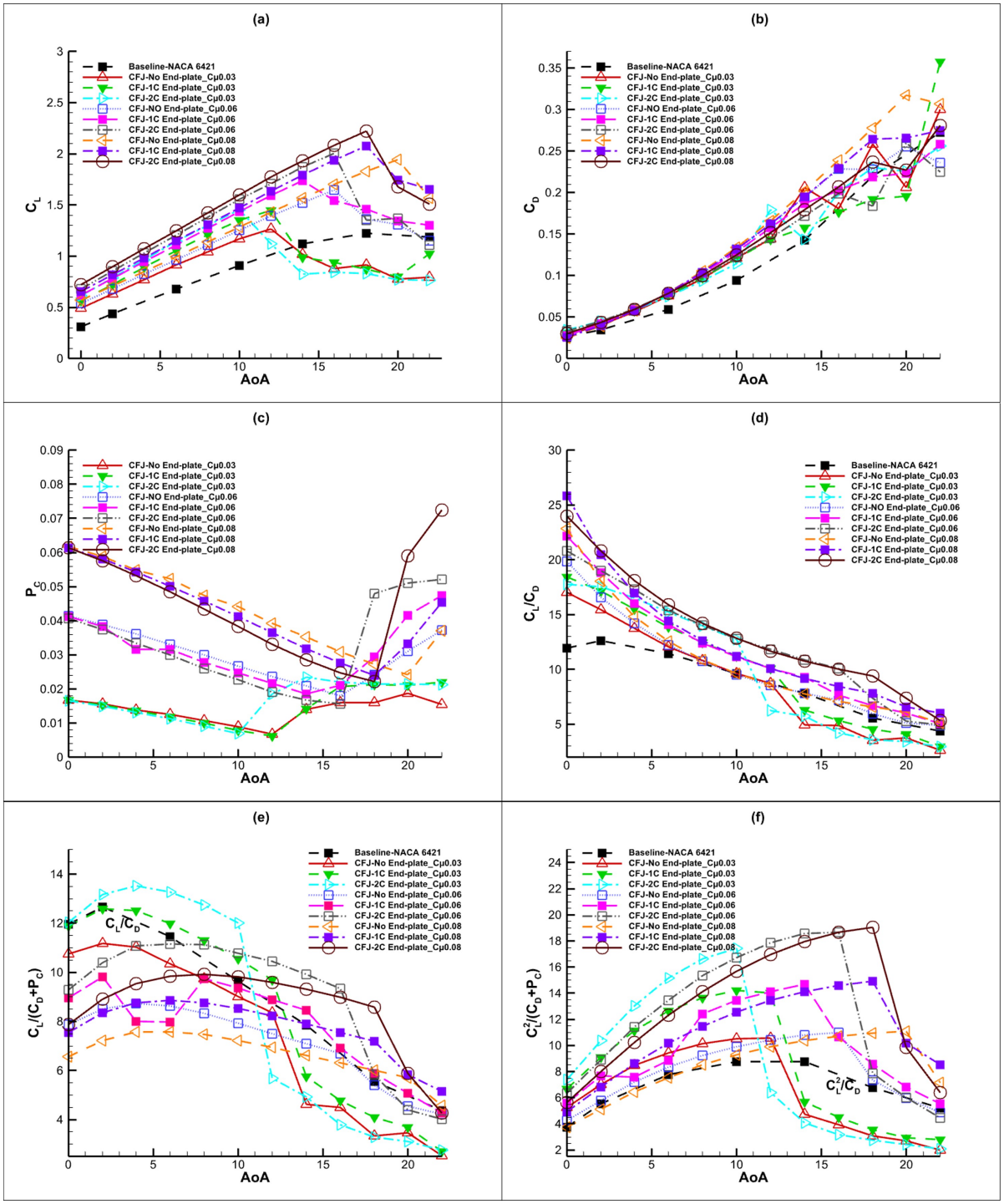

Figure 6: C_L, C_D, P_C, C_L/C_D, $(C_L/C_D)_c$ and $(C_L^2/C_D)_c$ for all configurations at different C_μ

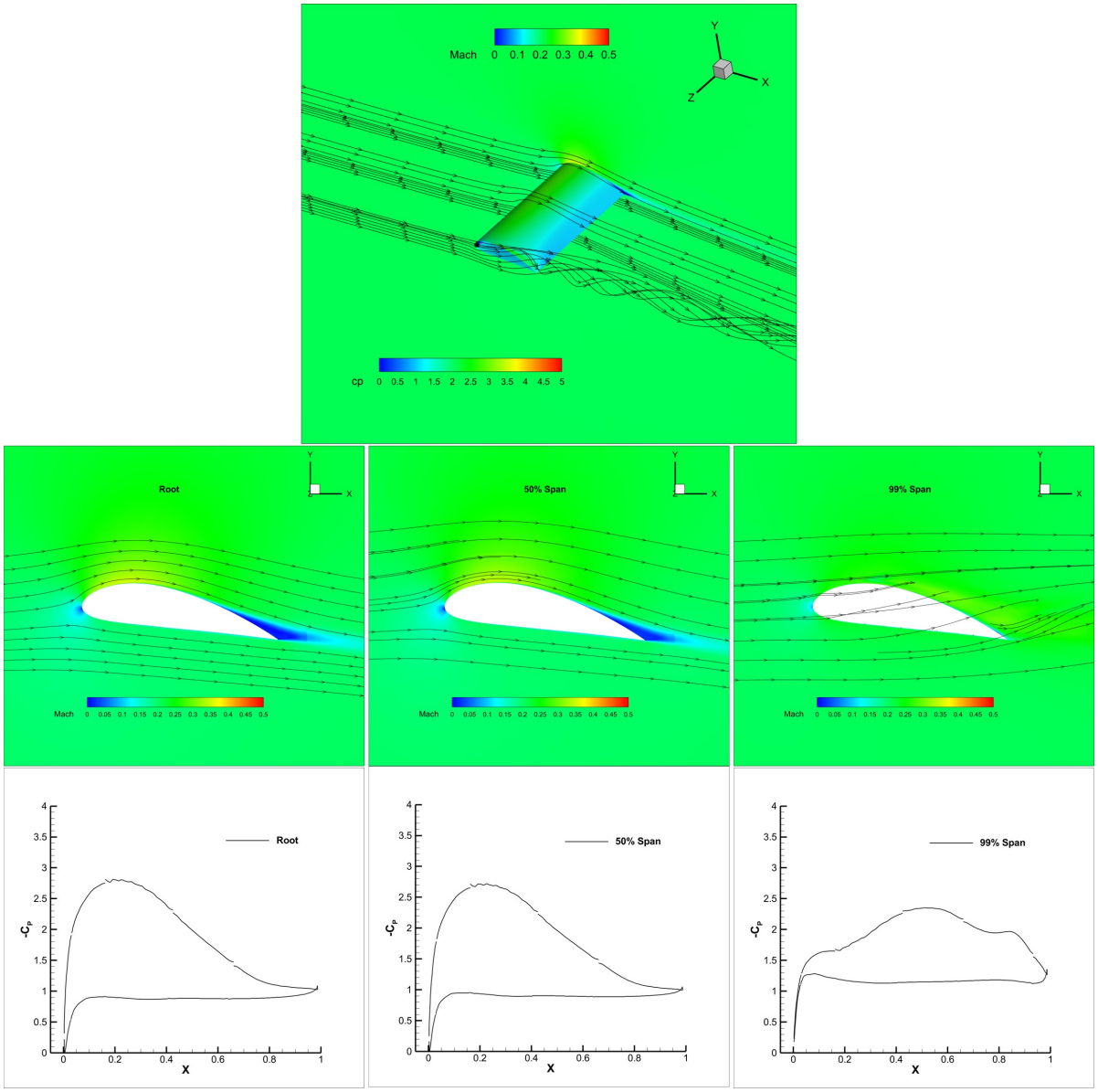

Figure 7: Baseline flow field and pressure coefficient at $AoA = 10°$

3.2 Results for CFJ Wing

3.2.1 CFJ Wing without End-Plates

Table. 3 summarizes the results of the 3D analysis of the CFJ wing with no end-plates across the AoA range at different C_μ values. Before the stall occurs, the average C_L is about 36% higher than that of the baseline airfoil under identical test conditions. Increasing the jet momentum favors these gains. With $C_\mu = 0.08$, $C_L = 1.83$ is attained at $\alpha = 18°$, a 50% rise over the maximum lift coefficient of baseline airfoils at the same AoA. Additionally, the maximum productivity efficiency $(C_L^2/C_D)_c$ of 11.08 is found under the same condition, which increased by 24.4% compared with the maximum C_L^2/C_D of 8.91 of

Table 2: Aerodynamic performance for Baseline Airfoils

AoA	C_L	C_D	C_L/C_D	C_L^2/C_D
0	0.312	0.026	11.96	3.73
2	0.436	0.034	12.65	5.51
4	0.559	0.046	12.27	6.85
6	0.679	0.059	11.46	7.78
8	0.798	0.076	10.54	8.41
10	0.911	0.094	9.64	8.78
12	1.015	0.116	8.78	8.91
14	1.120	0.143	7.84	8.78
16	1.178	0.176	6.70	7.89
18	1.221	0.220	5.56	6.79
20	1.211	0.250	4.85	5.87
22	1.190	0.272	4.37	5.20

baseline NACA 6421 wing.

The Mach contours and C_p distributions in Fig. 8 and Fig. 9, the trailing edge flow separation does not exit at AoA of 10° for both C_μ of 0.03 and 0.08. A strong spiraling tip vortex is still present near the tip of the wing. At the root and mid-span, the pressure coefficient distributions essentially overlap with one another, indicating that the primary efficiency losses originate near the tip region.

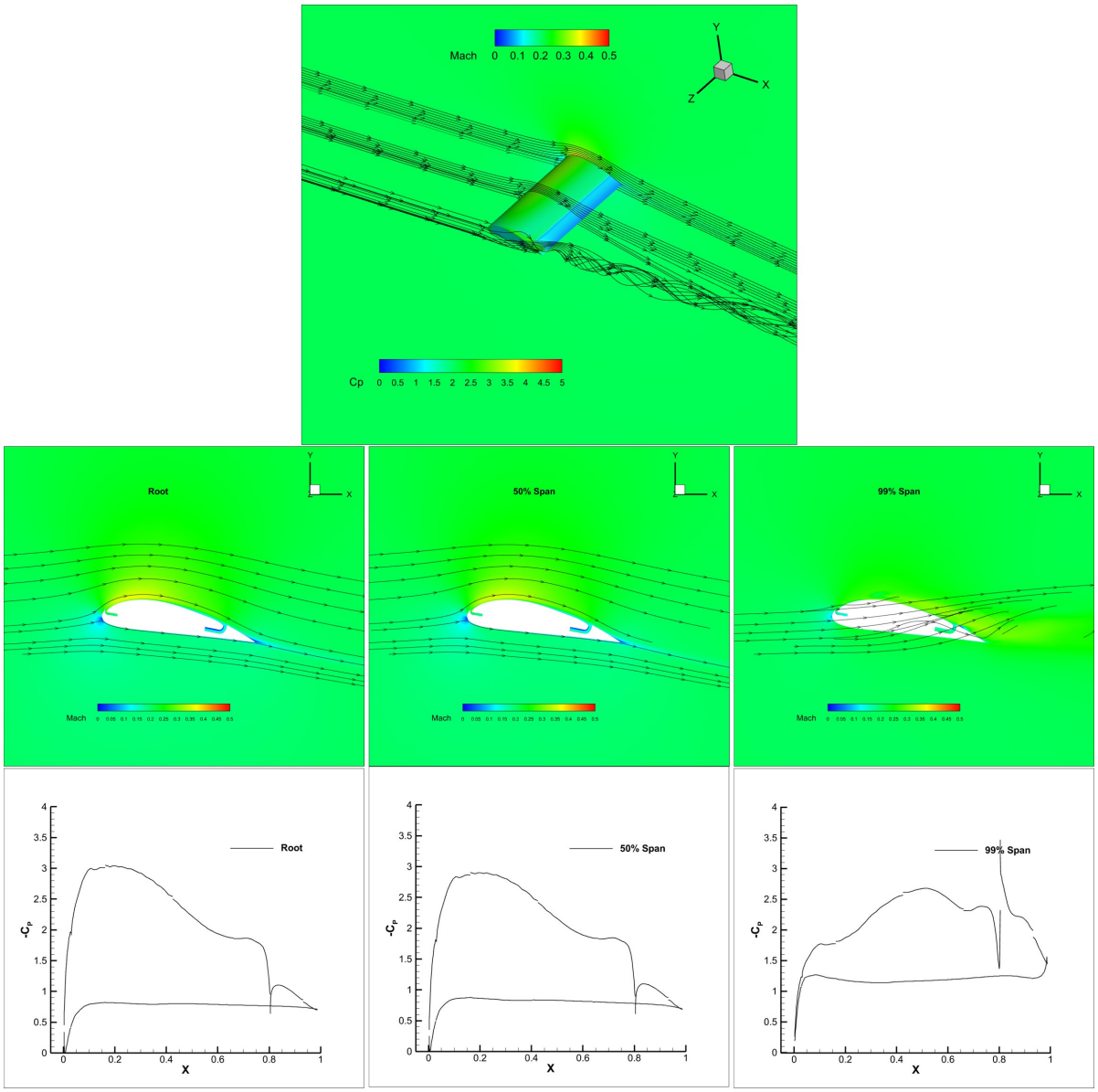

Figure 8: CFJ flow field and pressure coefficient at $C_\mu = 0.03$ and $AoA = 10°$

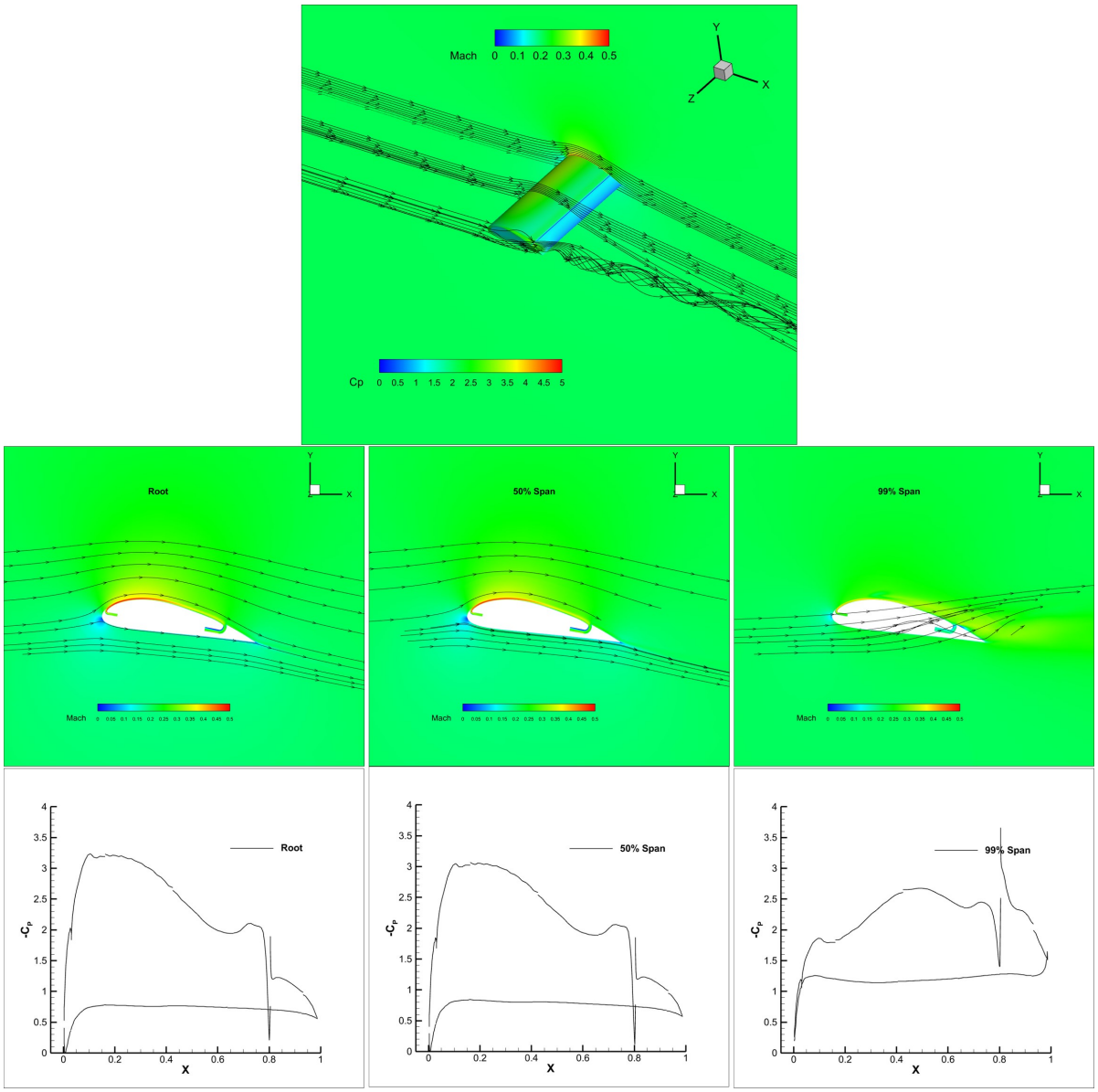

Figure 9: CFJ flow field and pressure coefficient at $C_\mu = 0.08$ and $AoA = 10°$

Table 3: CFJ Wings with No End-Plates Results

Metric	Angle of attack α (deg)											
	0	2	4	6	8	10	12	14	16	18	20	22
	$C_\mu = 0.03$											
C_L	0.49	0.63	0.77	0.91	1.04	1.17	1.26	1.02	0.88	0.91	0.78	0.79
C_D	0.029	0.041	0.056	0.075	0.096	0.121	0.144	0.206	0.180	0.258	0.206	0.300
C_L/C_D	17.01	15.43	13.75	12.09	10.81	9.66	8.74	4.94	4.88	3.54	3.77	2.65
Pt ratio	1.039	1.037	1.033	1.030	1.025	1.021	1.016	1.030	1.038	1.040	1.045	1.049
P_C	0.017	0.016	0.014	0.013	0.011	0.009	0.007	0.014	0.016	0.016	0.019	0.015
$(C_L/C_D)_c$	10.74	11.16	11.01	10.35	9.73	9.00	8.36	4.63	4.48	3.34	3.45	2.52
$(C_L^2/C_D)_c$	5.26	7.01	8.45	9.44	10.13	10.50	10.55	4.71	3.95	3.05	2.68	2.00
	$C_\mu = 0.06$											
C_L	0.54	0.68	0.82	0.96	1.11	1.25	1.39	1.52	1.65	1.36	1.31	1.15
C_D	0.027	0.041	0.058	0.079	0.103	0.131	0.162	0.194	0.228	0.228	0.256	0.236
C_L/C_D	19.83	16.60	14.18	12.22	10.74	9.53	8.58	7.84	7.21	5.98	5.11	4.88
Pt ratio	1.069	1.065	1.061	1.055	1.050	1.045	1.040	1.035	1.031	1.042	1.054	1.064
P_C	0.041	0.039	0.036	0.033	0.030	0.027	0.024	0.021	0.018	0.024	0.031	0.037
$(C_L/C_D)_c$	7.88	8.51	8.73	8.62	8.32	7.92	7.49	7.08	6.68	5.40	4.56	4.21
$(C_L^2/C_D)_c$	4.26	5.78	7.18	8.32	9.23	9.92	10.43	10.79	11.01	7.35	5.95	4.85
	$C_\mu = 0.08$											
C_L	0.57	0.71	0.85	1.00	1.14	1.28	1.43	1.57	1.70	1.83	1.94	1.57
C_D	0.025	0.039	0.057	0.079	0.105	0.134	0.166	0.202	0.239	0.277	0.317	0.306
C_L/C_D	22.82	18.07	14.84	12.57	10.86	9.61	8.59	7.77	7.12	6.59	6.13	5.12
Pt ratio	1.090	1.086	1.081	1.077	1.070	1.065	1.058	1.052	1.046	1.041	1.036	1.056
P_C	0.062	0.059	0.055	0.052	0.047	0.044	0.040	0.035	0.031	0.027	0.024	0.037
$(C_L/C_D)_c$	6.57	7.23	7.58	7.57	7.48	7.22	6.95	6.62	6.30	6.00	5.70	4.57
$(C_L^2/C_D)_c$	3.74	5.13	6.45	7.54	8.82	9.28	9.91	10.37	10.72	10.95	11.08	7.17

3.2.2 CFJ Wing with One-Chord End-Plates

Fig. 10 and Fig. 11 illustrate the flow field and C_P distribution at $AoA = 10°$ when one chord end-plates is installed at the tip of the wings at $C_\mu = 0.03$ and $C_\mu = 0.08$, respectively. These two flow field plots reveal that increasing the C_μ from 0.03 to 0.08 increases the C_P values at every spanwise location. Integrating this larger pressure difference raises the pre-stall average C_L of the $C_\mu = 0.08$ case by approximately 33.7%, and a 5.0% increase in maximum $(C_L^2/C_D)_c$ compared with the cases of $C_\mu = 0.03$ as shown in the Table. 4. Comparing to the CFJ wing with no end plate, a significant lift improvement is achieved at the near tip region as shown by the C_P distribution at 90% span, which is much closer to those at the inner span than the one with no end-plates shown in Fig. 8 and Fig. 9. The streamlines near the tip issued from the same location as those in Fig. 8 and Fig. 9 show little spiraling pattern, even though the streamlines are still lifted up due to the low pressure on the suction surface. The wing circulation vortex tube appears to be largely stopped by the circular end-plates, which makes the flow more two-dimensional.

Table. 4 presents the aerodynamic performance of the CFJ wing with 1C end-plate over the full AoA range and different C_μ settings. The average C_L of one-chord end-plates CFJ airfoil is increasing by about 20% compared to the CFJ wing with no end-plates, and by around 60% compared to the baseline wings with no end-plates. Because less spanwise leakage occurs, the CFJ can keep energizing the boundary layer all the way to the tip, delaying flow separation and raising the sectional lift there. That local improvement

answers why the overall lift coefficient, at a fixed momentum coefficient, increased significantly as shown in Fig. 12 (a). Fig. 12 (b) displays the C_D for CFJ with one chord end-plates at $C_\mu = 0.03$. It can be seen that the coefficient of drag roughly remains the same for all the CFJ wings with end-plates. The power coefficient drops slightly before the wing is near stall at high AoA.

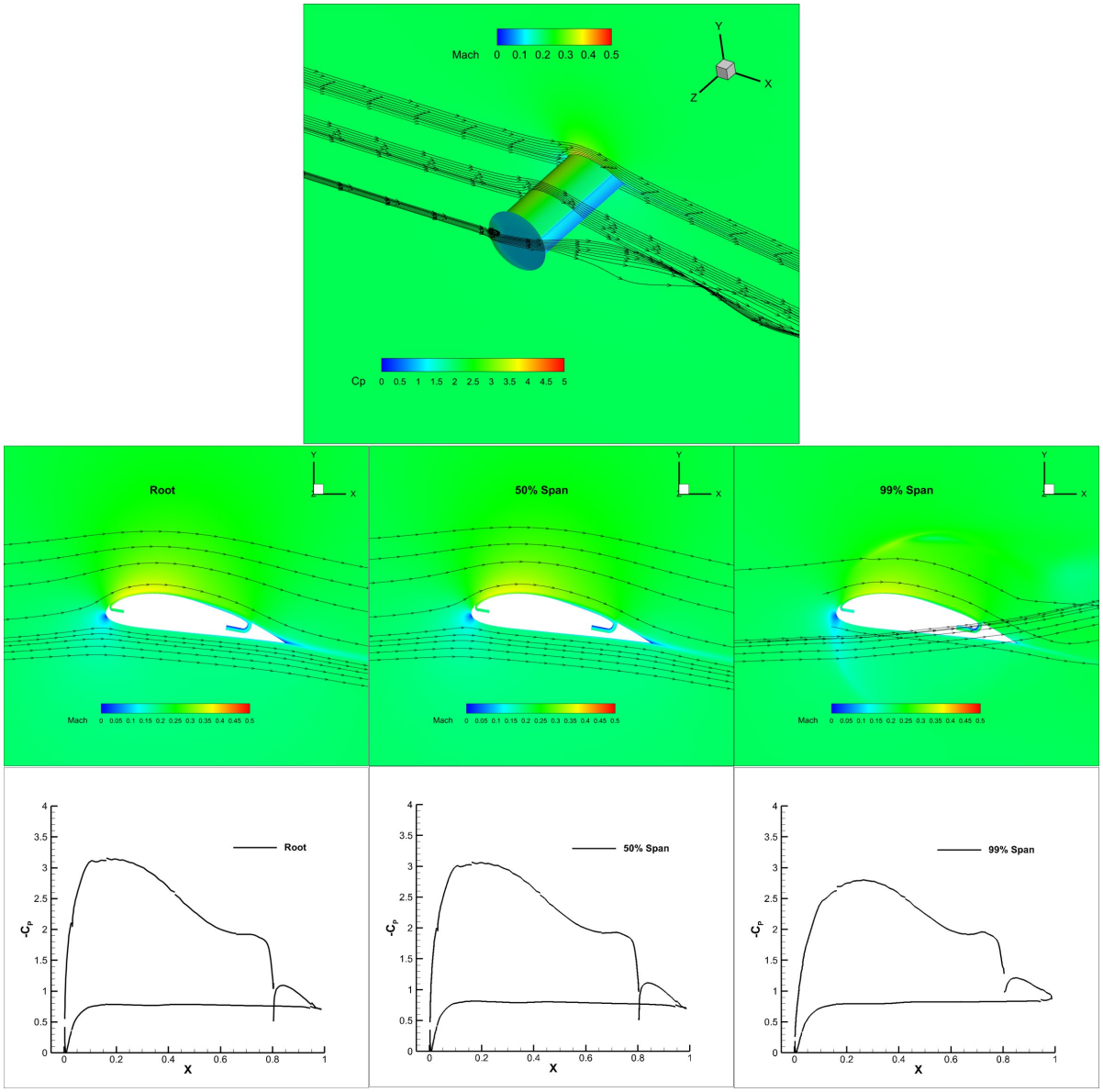

Figure 10: CFJ Wing with One Chord end-plates flow field and pressure coefficient at $C_\mu = 0.03$ and $AoA = 10°$

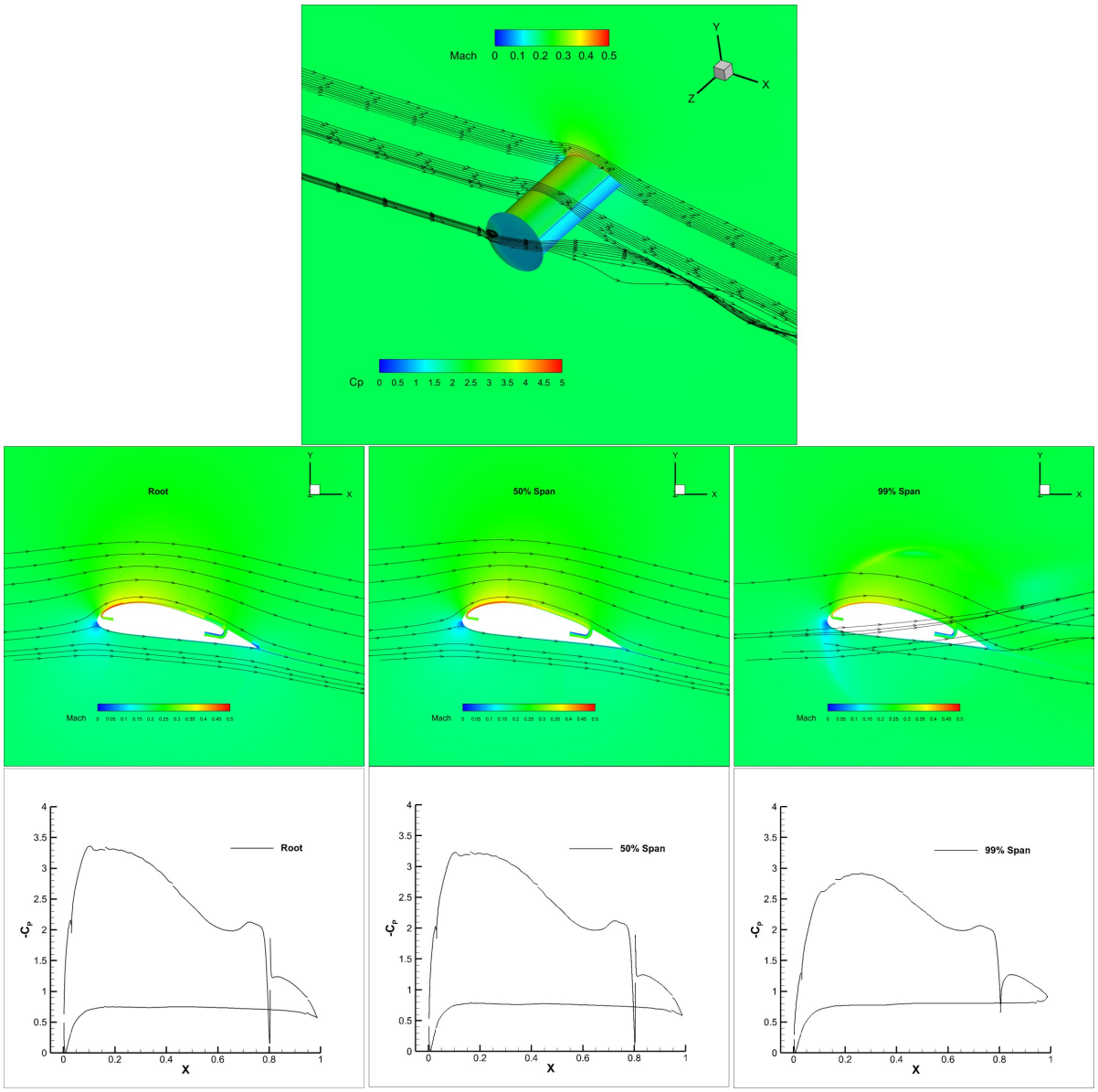

Figure 11: CFJ Wing with One Chord end-plates flow field and pressure coefficient at $C_\mu = 0.08$ and $AoA = 10^\circ$

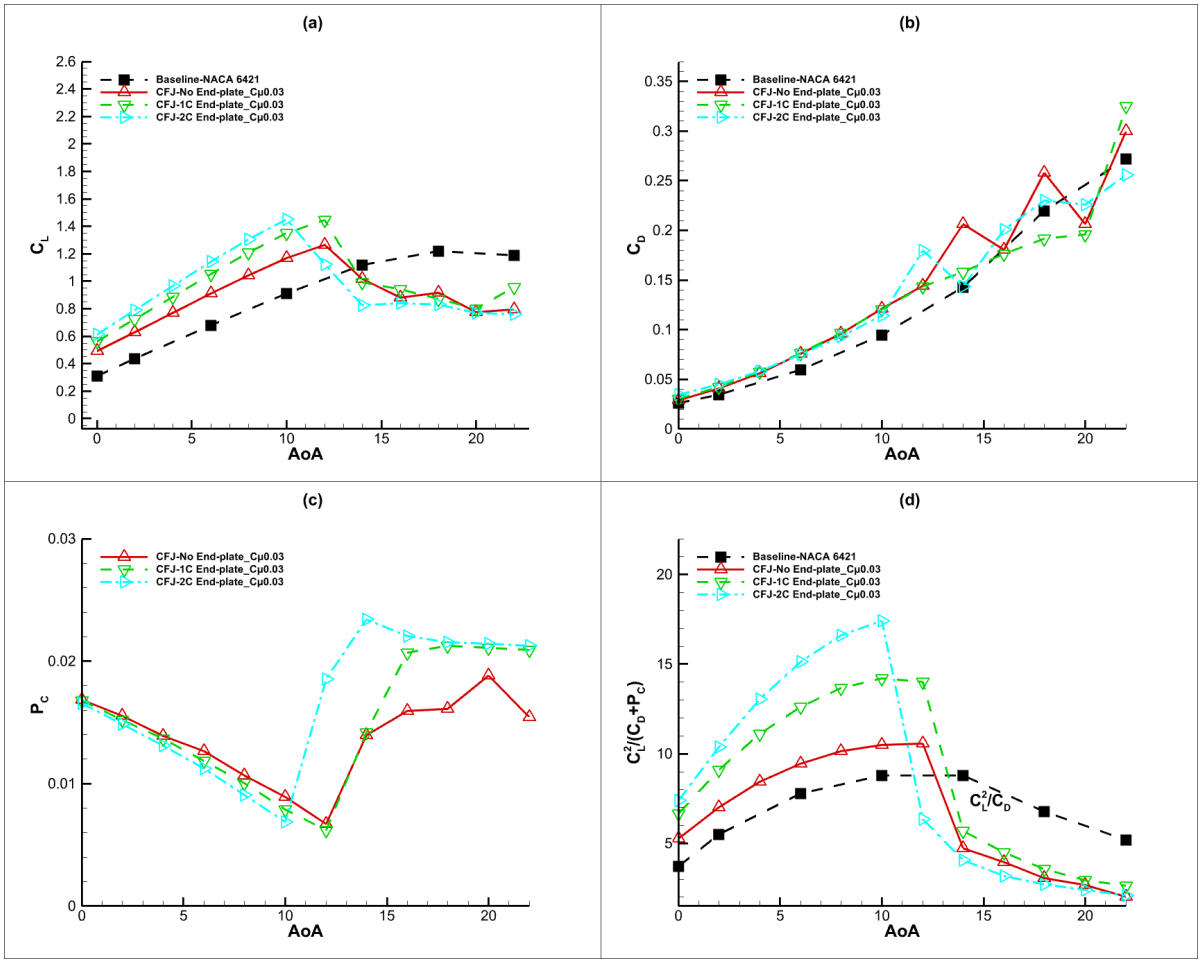

Figure 12: C_L, C_D, P_C, and $(C_L^2/C_D)_c$ for CFJ Wing with One Chord End-Plates at $C_\mu = 0.03$

Table 4: CFJ Wing with One-Chord End-Plates Results

Metric	Angle of attack α (deg)											
	0	2	4	6	8	10	12	14	16	18	20	22
	$C_\mu = 0.03$											
C_L	0.56	0.72	0.89	1.05	1.21	1.35	1.45	0.99	0.94	0.87	0.80	1.03
C_D	0.030	0.042	0.057	0.076	0.097	0.120	0.143	0.158	0.176	0.192	0.196	0.357
C_L/C_D	18.42	17.12	15.51	13.85	12.46	11.23	10.09	6.27	5.33	4.54	4.08	2.87
P_C	0.017	0.015	0.014	0.012	0.010	0.008	0.006	0.014	0.021	0.021	0.021	0.022
Pt ratio	1.039	1.036	1.032	1.028	1.024	1.019	1.015	1.039	1.050	1.052	1.051	1.051
$(C_L/C_D)_c$	11.88	12.59	12.52	11.98	11.30	10.53	9.68	5.76	4.77	4.09	3.68	2.71
$(C_L^2/C_D)_c$	6.67	9.11	11.12	12.64	13.65	14.22	14.00	5.70	4.49	3.56	2.94	2.78
	$C_\mu = 0.06$											
C_L	0.62	0.78	0.95	1.11	1.27	1.44	1.59	1.74	1.54	1.46	1.34	1.30
C_D	0.028	0.042	0.059	0.079	0.103	0.129	0.158	0.187	0.202	0.219	0.223	0.258
C_L/C_D	22.14	18.85	15.99	14.09	12.39	11.16	10.09	9.29	7.63	6.68	6.03	5.04
P_C	0.041	0.038	0.059	0.060	0.028	0.025	0.022	0.019	0.021	0.029	0.042	0.047
Pt ratio	1.069	1.064	1.058	1.053	1.047	1.042	1.037	1.032	1.036	1.051	1.073	1.083
$(C_L/C_D)_c$	8.97	9.82	7.99	7.97	9.75	9.36	8.88	8.45	6.91	5.89	5.08	4.26
$(C_L^2/C_D)_c$	5.56	7.69	7.56	8.84	12.41	13.43	14.12	14.67	10.65	8.59	6.83	5.55
	$C_\mu = 0.08$											
C_L	0.65	0.82	0.98	1.15	1.31	1.47	1.63	1.79	1.93	2.07	1.74	1.65
C_D	0.025	0.040	0.058	0.079	0.104	0.131	0.162	0.195	0.229	0.265	0.266	0.275
C_L/C_D	25.83	20.48	16.98	14.44	12.60	11.22	10.10	9.18	8.45	7.84	6.57	6.01
P_C	0.061	0.058	0.054	0.050	0.046	0.041	0.036	0.032	0.028	0.024	0.033	0.045
Pt ratio	1.090	1.085	1.079	1.073	1.067	1.060	1.054	1.047	1.041	1.036	1.050	1.069
$(C_L/C_D)_c$	7.54	8.35	8.77	8.86	8.75	8.54	8.24	7.89	7.54	7.19	5.83	5.15
$(C_L^2/C_D)_c$	4.93	6.84	8.62	10.17	11.47	12.57	13.45	14.12	14.58	14.92	10.18	8.51

3.2.3 CFJ Wing with Two-Chords End-Plates

Fig. 13 and Fig. 14 show that the 2C end-plate further mitigates the tip vortex effect and makes the wing tip flow even closer to the inner span than that of the 1C plate.

Table. 5 displays the aerodynamic results of the CFJ wing with 2C end-plates across the full angles of attack range and different jet momentum. It is observed that the 2C end-plate continues to increase the lift coefficient and decrease the drag coefficient. For the $C_\mu = 0.08$, the wing reaches a lift coefficient of $C_L = 2.22$ at $\alpha = 18°$, which is about 8.5% higher than the one chord case. The C_D drops from 0.265 to 0.237, and the power coefficient slightly falls to 0.022. As a result, a substantial increase of the productivity efficiency $(C_L^2/C_D)_c$ by 28% is achieved compared to the 1C end-plate.

Fig. 15 presents the results of the 2C end-plate for $C_\mu = 0.03, 0.06$, and 0.08, shows the lift curves move up with the increasing jet strength. From $C_\mu = 0.03$ to $C_\mu = 0.06$, the stall AoA is increased from 10° to 16°. For $(C_L^2/C_D)_c$, in Fig. 15 (d), it indicates that at low AoA, C_μ of 0.03 is preferred since higher C_μ does not bring a lot of productivity efficiency gain. At higher AoA when the low C_μ can not avoid stall, increasing C_μ is efficient and effective to increase the stall AoA and operation range.

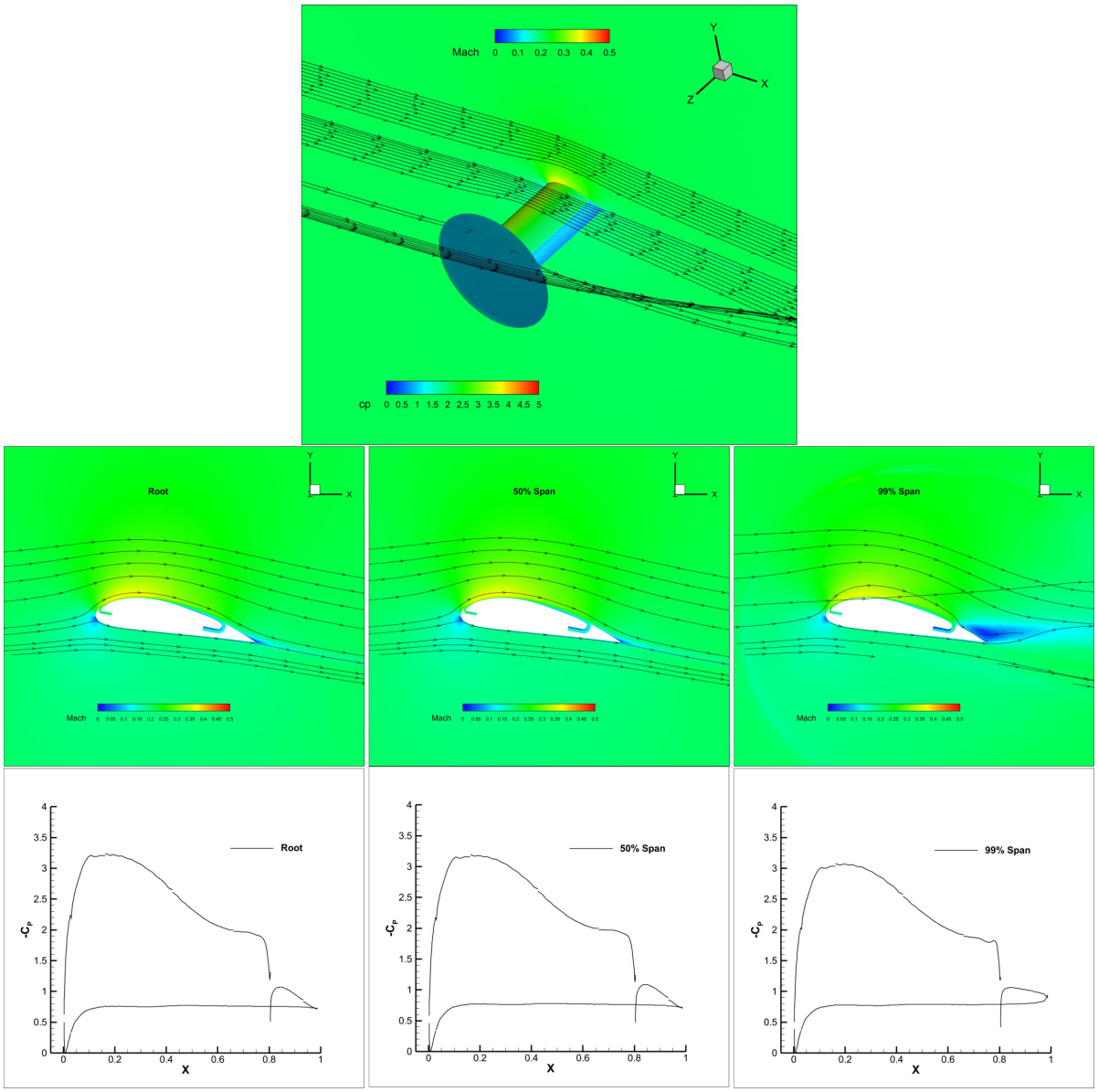

Figure 13: CFJ Wing with Two Chords end-plates flow field and pressure coefficient at $C_\mu = 0.03$ and $AoA = 10^\circ$

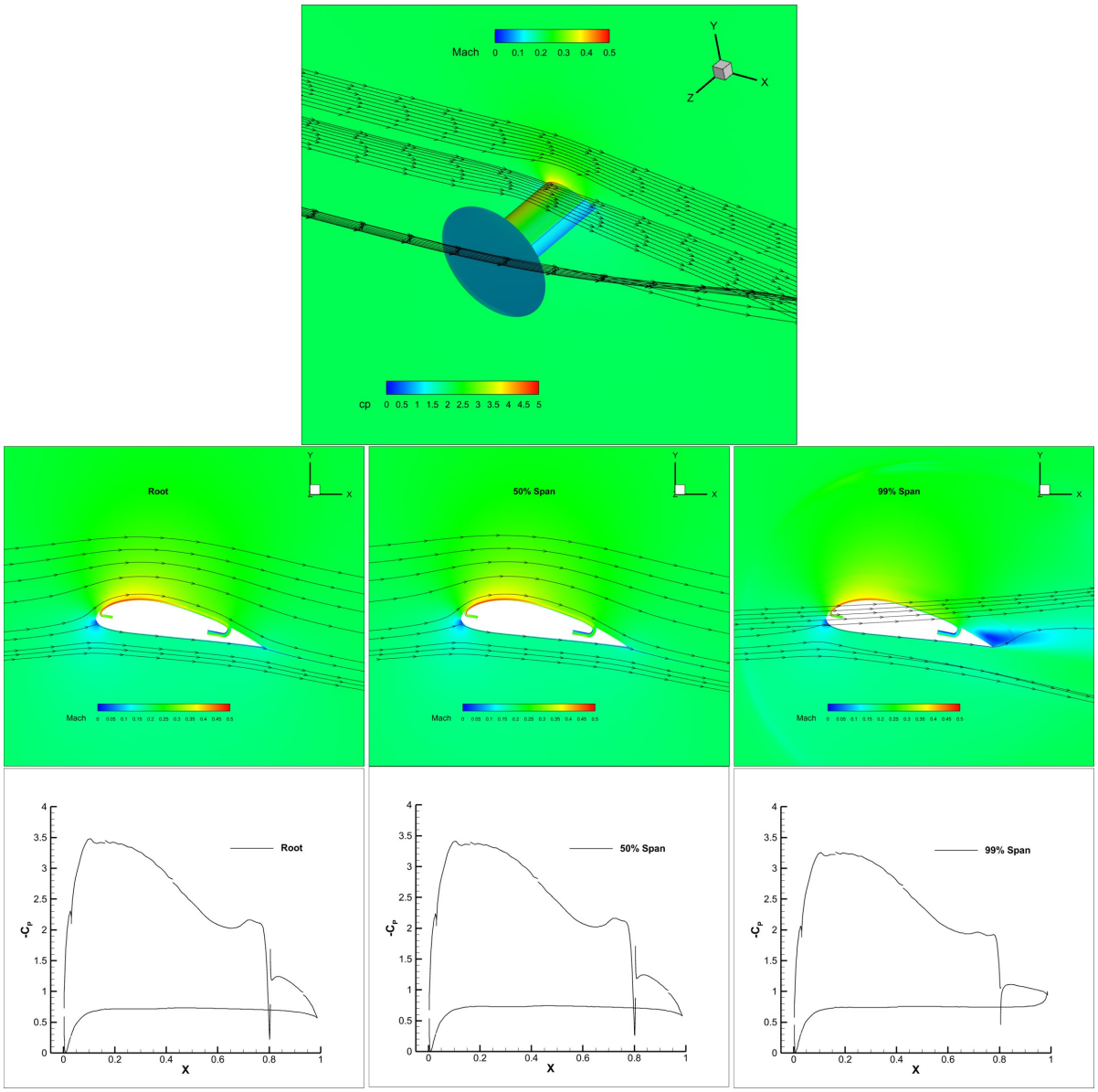

Figure 14: CFJ Wing with Two Chords end-plates flow field and pressure coefficient at $C_\mu = 0.08$ and $AoA = 10^\circ$

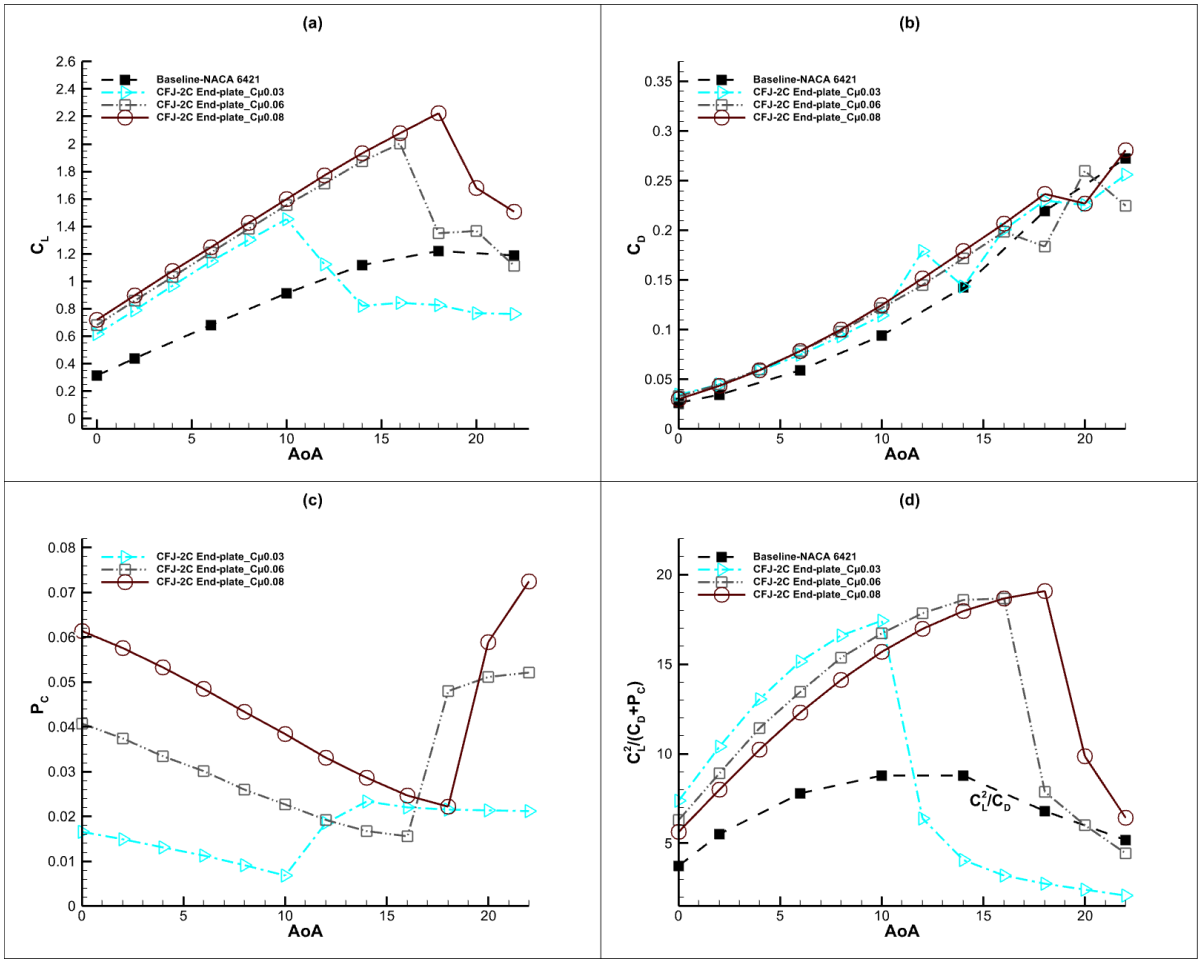

Figure 15: C_L, C_D, P_C, and $(C_L^2/C_D)_c$ for all the designs at $C_\mu = 0.03$ and $C_\mu = 0.08$

Table 5: CFJ Wing with Two-Chords End-Plates Results

Metric	Angle of attack α (deg)											
	0	2	4	6	8	10	12	14	16	18	20	22
	$C_\mu = 0.03$											
C_L	0.61	0.79	0.97	1.14	1.30	1.45	1.12	0.82	0.84	0.83	0.77	0.76
C_D	0.035	0.045	0.058	0.075	0.093	0.114	0.180	0.144	0.201	0.230	0.226	0.256
C_L/C_D	17.78	17.52	16.54	15.24	13.98	12.73	6.26	5.73	4.20	3.60	3.41	2.97
P_C	0.017	0.015	0.013	0.011	0.009	0.007	0.019	0.023	0.022	0.022	0.021	0.021
Pt ratio	1.039	1.035	1.031	1.027	1.022	1.016	1.045	1.056	1.053	1.052	1.052	1.052
$(C_L/C_D)_c$	12.02	13.17	13.51	13.26	12.74	12.01	5.67	4.93	3.78	3.30	3.11	2.75
$(C_L^2/C_D)_c$	7.38	10.38	13.05	15.15	16.61	17.41	6.37	4.06	3.19	2.73	2.40	2.09
	$C_\mu = 0.06$											
C_L	0.68	0.86	1.03	1.21	1.38	1.55	1.71	1.87	2.00	1.35	1.37	1.11
C_D	0.033	0.045	0.060	0.078	0.098	0.122	0.145	0.172	0.199	0.184	0.259	0.225
C_L/C_D	20.82	19.00	17.30	15.42	14.06	12.78	11.83	10.89	10.07	7.35	5.27	4.95
P_C	0.041	0.037	0.033	0.030	0.026	0.023	0.019	0.017	0.016	0.048	0.051	0.052
Pt ratio	1.068	1.063	1.056	1.051	1.044	1.039	1.033	1.029	1.027	1.084	1.090	1.091
$(C_L/C_D)_c$	9.28	10.39	11.08	11.14	11.12	10.76	10.44	9.92	9.33	5.83	4.41	4.01
$(C_L^2/C_D)_c$	6.32	8.90	11.41	13.46	15.34	16.71	17.85	18.57	18.68	7.88	6.03	4.46
	$C_\mu = 0.08$											
C_L	0.72	0.90	1.07	1.25	1.42	1.60	1.77	1.93	2.08	2.22	1.68	1.50
C_D	0.030	0.043	0.059	0.079	0.100	0.125	0.152	0.179	0.207	0.237	0.227	0.281
C_L/C_D	23.98	20.79	18.09	15.92	14.20	12.82	11.66	10.78	10.05	9.39	7.39	5.36
P_C	0.061	0.058	0.053	0.048	0.043	0.038	0.033	0.029	0.025	0.022	0.059	0.072
Pt ratio	1.089	1.084	1.078	1.071	1.064	1.056	1.049	1.043	1.037	1.034	1.095	1.111
$(C_L/C_D)_c$	7.86	8.90	9.54	9.84	9.91	9.81	9.58	9.30	8.98	8.58	5.87	4.26
$(C_L^2/C_D)_c$	5.65	7.99	10.25	12.30	14.13	15.67	16.97	17.95	18.67	19.06	9.86	6.41

4 Conclusion

This study numerically investigates the cruise performance improvement of CFJ wings with circular end-plates for a CFJ wing based on NACA 6421 airfoil with an aspect ratio of 4 at $Re = 1 \times 10^6$ and $M = 0.211$. Three wing tip treatments were modeled, no plate, 1C and 2C end-plate, over an AoA range of $\alpha = 0^\circ \sim 22^\circ$ and jet-momentum coefficients $C_\mu = 0.03$, 0.06, 0.08.

Compared to the baseline airfoils, whose maximum lift coefficient is $C_{L,\max} = 1.221$ and whose highest productivity efficiency $(C_L^2/C_D)_c$ is only 8.9, using CFJ alone would raise pre-stall lift by about one-third with $C_L = 1.83$ and a productivity efficiency of 11.4 at $\alpha = 18^\circ$ and $C_\mu = 0.08$.

Using 1C circular end-plates is very effective to mitigate the tip vortex with little flow spiraling. The flow along the span is more 2-dimensional. The averaged lift coefficient is increased by 20% compared to the CFJ wing with no end-plates. At $\alpha = 18^\circ$ this configuration reaches $C_L = 2.07$ and $(C_L^2/C_D)_c$ of 14.9—about 70 % above the baseline and 30 % above the CFJ airfoils with no end-plates.

Increasing the plate diameter to 2C almost eliminates tip-vortex influence. Spanwise pressure coefficient distribution is fairly uniform. At C_μ of 0.08, the wing attains $C_L = 2.22$, $C_D = 0.237$ and $P_c = 0.022$, yielding a cruise productivity efficiency of 19.1. For cruise at $AoA < 10^\circ$, C_μ of 0.03 is desirable since higher C_μ does not bring a lot of productivity efficiency gain. At higher AoA when the low C_μ can not

avoid stall, increasing C_μ is efficient and effective to increase the stall AoA and operation range.

In summary, the circular end-plate is very effective in mitigating tip vortex and improving a CFJ wing's lift coefficient, aerodynamic efficiency, and productivity efficiency. The 2C end-plate is even more effective and virtually eliminates the tip vortex effect.

5 Acknowledgment

The authors would like to acknowledge the computing resources provided by the Center of Computational Sciences (CCS) at the University of Miami. The teaching assistantship support from the University of Miami is also acknowledged.

Disclosure: The University of Miami and Dr. Gecheng Zha may receive royalties for future commercialization of the intellectual property used in this study. The University of Miami is also equity owner in CoFlow Jet, LLC, licensee of the intellectual property used in this study.

References

[1] R. T. Whitcomb, "A design approach and selected wind tunnel results at high subsonic speeds for wing-tip mounted winglets," tech. rep., 1976.

[2] H. Helal, E. E. Khalil, O. E. Abdellatif, and G. M. Elhariry, "Aerodynamic analyses of aircraft-blended winglet performance," *IOSR J. Mech. Civ. Eng. Ver*, vol. 13, no. 3, pp. 2320–334, 2016.

[3] Zha, G.-C,, "Feasibility Study of Deflected Slipstream Airfoil for VTOL Hover Enabled by CoFlow Jet," *Proceedings of AIAA Aviation Forum 2023, 12–16 June 2023, San Diego, CA*, 2023.

[4] G.-C. Zha, Y. Ren, and W. Fredericks, "Design and Testing of Deflected Slipstream Airfoil for VTOL Hover Enabled by CoFlow Jet." AIAA Paper 2024-4420, 2024 AIAA AVIATION Forum and 2024 ASCEND, Las Vegas, NV, 29 July–2 August 2024.

[5] P. E. Hemke, *Drag of wings with end plates*, vol. 267. US Government Printing Office, 1927.

[6] G.-C. Zha and D. C. Paxton, "A Novel Flow Control Method for Airfoil Performance Enhancement Using Co-Flow Jet." *Applications of Circulation Control Technologies*, Chapter 10, p. 293-314, Vol. 214, Progress in Astronautics and Aeronautics, AIAA Book Series, Editors: Joslin, R. D. and Jones, G.S., 2006.

[7] G.-C. Zha, W. Gao, and C. Paxton, "Jet Effects on Co-Flow Jet Airfoil Performance," *AIAA Journal, No. 6,*, vol. 45, pp. 1222–1231, 2007.

[8] G.-C. Zha, C. Paxton, A. Conley, A. Wells, and B. Carroll, "Effect of Injection Slot Size on High Performance Co-Flow Jet Airfoil," *AIAA Journal of Aircraft*, vol. 43, 2006.

[9] G.-C. Zha, B. Carroll, C. Paxton, A. Conley, and A. Wells, "High Performance Airfoil with Co-Flow Jet Flow Control," *AIAA Journal*, vol. 45, 2007.

[10] Wang, B.-Y. and Haddoukessouni, B. and Levy, J. and Zha, G.-C., "Numerical Investigations of Injection Slot Size Effect on the Performance of Co-Flow Jet Airfoil," *Journal of Aircraft*, vol. Vol. 45, No. 6,, pp. pp.2084–2091, 2008.

[11] B. P. E. Dano, D. Kirk, and G.-C. Zha, "Experimental Investigation of Jet Mixing Mechanism of Co- Flow Jet Airfoil." AIAA-2010-4421, 5th AIAA Flow Control Conference, Chicago, IL, 28 Jun - 1 Jul 2010.

[12] B. P. E. Dano, G.-C. Zha, and M. Castillo, "Experimental Study of Co-Flow Jet Airfoil Performance Enhancement Using Micro Discrete Jets." AIAA Paper 2011-0941, 49th AIAA Aerospace Sciences Meeting, Orlando, FL, 4-7 January 2011.

[13] A. Lefebvre, B. Dano, W. Bartow, M. Fronzo, and G. Zha, "Performance and energy expenditure of coflow jet airfoil with variation of mach number," *Journal of Aircraft*, vol. 53, no. 6, pp. 1757–1767, 2016.

[14] A. Lefebvre, G-C. Zha, "Numerical Simulation of Pitching Airfoil Performance Enhancement Using Co-Flow Jet Flow Control," *AIAA paper 2013-2517*, June 2013.

[15] A. Lefebvre, G-C. Zha, "Co-Flow Jet Airfoil Trade Study Part I : Energy Consumption and Aerodynamic Performance," *Proceedings of the AIAA Flow Control Conference*, June 2014.

[16] A. Lefebvre, G-C. Zha, "Co-Flow Jet Airfoil Trade Study Part II : Moment and Drag," *Proceedings of the AIAA Flow Control Conference*, June 2014.

[17] Yunchao Yang, Gecheng Zha, "Super-Lift Coefficient of Active Flow Control Airfoil: What is the Limit?," *AIAA Paper 2017-1693, AIAA SCITECH2017, 55th AIAA Aerospace Science Meeting, Grapevine, Texas, 9-13 January 2017*, 2017.

[18] Gecheng Zha, Yunchao Yang, Yan Ren, Brendan McBreen, "Super-Lift and Thrusting Airfoil of Coflow Jet Actuated by Micro-Compressors," *AIAA Paper-2018-3061, AIAA AVIATION Forum 2018, Flow Control Conference, June 25-29*, 2018.

[19] Lefebvre, A. and Zha, G.-C., "Trade Study of 3D Co-Flow Jet Wing for Cruise Performance." AIAA Paper 2016-0570, AIAA SCITECH2016, AIAA Aerospace Science Meeting, San Diego, CA, 4-8 January 2016.

[20] Kewei Xu, Gecheng Zha, "High Control Authority 3D Aircraft Control Surfaces Using Co-Flow Jet," *AIAA Journal of Aircraft*, 2020.

[21] Kewei Xu, Yan Ren, Gecheng Zha, "Numerical Analysis of Energy Expenditure for Co-Flow Wall Jet Separation Control," *AIAA Journal, published online: 11 Jan 2022, doi.org/10.2514/1.J061015*, 2022.

[22] Yang Wang and Gecheng Zha, "Study of Mach Number Effect for 2D Co-Flow Jet Airfoil at Cruise Conditions," *AIAA Paper 2019-3169, AIAA Aviation 2019 Forum, 17-21 June 2019, Dallas, Texas*, 2019.

[23] Yang Wang and Gecheng Zha, "Study of Mach Number Effect for 3D Co-Flow Jet Wings at Cruise Conditions," *AIAA Paper 2020-0045, AIAA SciTech Forum, 6-10 January 2020, Orlando, FL*, 2020.

[24] Y.-Q. Shen and G.-C. Zha, "Large Eddy Simulation Using a New Set of Sixth Order Schemes for Compressible Viscous Terms ," *Journal of Computational Physics*, vol. 229, pp. 8296–8312, 2010.

[25] Zha, G.C., Shen, Y.Q. and Wang, B.Y., "An improved low diffusion E-CUSP upwind scheme ," *Journal of Computer and Fluids*, vol. 48, pp. 214–220, Sep. 2011.

[26] Y.-Q. Shen and G.-Z. Zha , "Generalized finite compact difference scheme for shock/complex flowfield interaction," *Journal of Computational Physics*, vol. doi:10.1016/j.jcp.2011.01.039, 2011.

[27] Shen, Y.-Q. and Zha, G.-C. and Wang, B.-Y., " Improvement of Stability and Accuracy of Implicit WENO Scheme," *AIAA Journal*, vol. 47, No. 2, pp. 331–344, 2009.

[28] Shen, Y.-Q. and Zha, G.-C. and Chen, X.-Y., " High Order Conservative Differencing for Viscous Terms and the Application to Vortex-Induced Vibration Flows," *Journal of Computational Physics*, vol. 228(2), pp. 8283–8300, 2009.

[29] Shen, Y.-Q. and Zha, G.-C. , " Improvement of the WENO Scheme Smoothness Estimator," *International Journal for Numerical Methods in Fluids*, vol. DOI:10.1002/fld.2186, 2009.

[30] G.-C. Zha and E. Bilgen, "Numerical Study of Three-Dimensional Transonic Flows Using Unfactored Upwind-Relaxation Sweeping Algorithm," *Journal of Computational Physics*, vol. 125, pp. 425–433, 1996.

[31] B.-Y. Wang and G.-C. Zha, "A General Sub-Domain Boundary Mapping Procedure For Structured Grid CFD Parallel Computation," *AIAA Journal of Aerospace Computing, Information, and Communication*, vol. 5, No.11, pp. 2084–2091, 2008.

[32] Y.-Q. Shen, G.-C. Zha, and B.-Y. Wang, "Improvement of Stability and Accuracy of Implicit WENO Scheme ," *AIAA Journal*, vol. 47, pp. 331–344, 2009.

[33] D. R. Riley, "Wind-tunnel investigation and analysis of the effects of end plates on the aerodynamic characteristics of an unswept wing," Tech. Rep. TN 2440, 1951.

[34] Jaehyoung Jeon, Brendan McBreen, Yan Ren, and Gecheng Zha, "Study of 3D Flapped CoFlow Jet Wings for Ultra-High Cruise Lift Coefficient," *AIAA Aviation Forum, June 12-16*, 2023.